NANO LETTERS

Open Access
This article is licensed under CC-BY 4.0

pubs.acs.org/NanoLett
Letter

Electric-Field Tunable Anisotropic *g*-Factor Induced by Spin Pumping

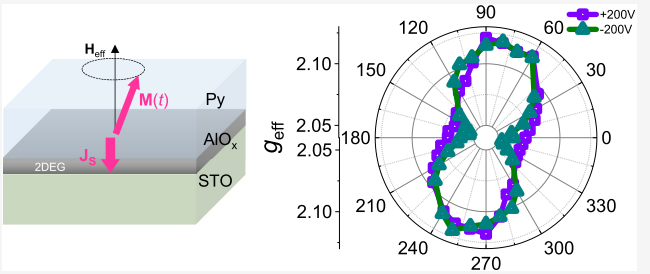
Jian Shao, Matthias Kronseder, Jianping Guo, Maximilian Mangold, Dong Pan, Thomas N. G. Meier, Weiwei Zhao,* Jianhua Zhao, Christian H. Back, and Lin Chen*

Cite This: *Nano Lett.* 2026, 26, 2853−2860

Read Online

ACCESS | Metrics & More | Article Recommendations | Supporting Information

ABSTRACT: Spin pumping, a well-established phenomenon where the precessing magnetization of a ferromagnet (FM) injects a pure spin current into an adjacent nonmagnetic layer, is characteristically identified by the enhancement of magnetic damping in the FM. Theoretical work has also suggested that spin pumping can affect the Landé *g*-factor—another key parameter of ferromagnetic materials besides the magnetic damping. However, experimental evidence of this effect has remained limited. Here, we demonstrate that spin pumping can lead to significant modulation of the *g*-factor in a Py/AlO_x/STO two-dimensional electron gas (2DEG) system with strong spin−orbit interaction. Specifically, we observe an anisotropic *g*-factor with 2-fold symmetry below the onset temperature of the 2DEG, and furthermore this anisotropy can be tuned when applying an external electric field. This work uncovers a previously overlooked effect and offers new possibilities for controlling magnetization dynamics in systems with a reduced dimension.



KEYWORDS: *spin pumping, 2DEG, Landé g-factor, spin−orbit interaction, electric-field control of magnetism*

The magnetization dynamics of a ferromagnet (FM) is determined by the phenomenological Landau-Lifshitz-Gilbert equation[1]

$$\frac{d\mathbf{M}}{dt} = -\gamma\mathbf{M}\times\mu_0\mathbf{H}_{\text{eff}} + \frac{\alpha}{M}\mathbf{M}\times\frac{d\mathbf{M}}{dt} \tag{1}$$

where $\mathbf{M}$ is the magnetization, t the time, γ (= $g\mu_B/\hbar$) the gyromagnetic ratio, g the Landé *g*-factor, μ_B the Bohr magneton, $\hbar$ the reduced Planck constant, μ_0 the magnetic constant, $\mathbf{H}_{\text{eff}}$ the effective magnetic-field, and α the damping constant of the FM. In FM/heavy metal (HM) bilayers, the magnetization dynamics of FM pumps spin currents that carry angular momentum and energy into the adjacent HM. The angular momentum relaxes due to the strong spin−orbit interaction (SOI) in the HM and leads to an enhancement of the damping in comparison with pure FM.[2,3] According to the theory of spin pumping, the modified damping α_{eff} is given by[2,4]

$$\alpha_{\text{eff}} = \frac{g_{\text{eff}}}{g}\left[\alpha + \frac{\hbar\gamma}{4\pi Mt}\text{Re}(g^{\uparrow\downarrow})\right] \tag{2}$$

where t is the thickness of FM, $\text{Re}(g^{\uparrow\downarrow})$ (always positive) the real part of the complex mixing conductance $g^{\uparrow\downarrow}$ at the FM/HM interface, and g_{eff} the modified the Landé *g*-factor by spin pumping. The magnitude of g_{eff} is expressed as[2,4]

$$g_{\text{eff}} = g\left[1 + \frac{\hbar\gamma}{4\pi Mt}\text{Im}(g^{\uparrow\downarrow})\right] \tag{3}$$

where $\text{Im}(g^{\uparrow\downarrow})$ is the imaginary part of $g^{\uparrow\downarrow}$. For ohmic FM/HM interfaces, first-principal calculations show that the sign of $\text{Im}(g^{\uparrow\downarrow})$ depends on the details of the structure (e.g., thickness as well as the choice of FM) but the magnitude of $|\text{Im}(g^{\uparrow\downarrow})|$ is about one order smaller than $\text{Re}(g^{\uparrow\downarrow})$.[4−10] Therefore, it is generally believed that $\text{Im}(g^{\uparrow\downarrow})$ is negligibly small and there is no modulation of *g*-factor in FM/HM bilayers.

On the other hand, the reciprocal effect of spin pumping is the current-induced spin−orbit torques in FM/HM bilayers, where a dc current in HM generates additional damping-like $\boldsymbol{\tau}_{\text{DL}}$ and field-like $\boldsymbol{\tau}_{\text{FL}}$ torques acting on the FM.[11] The spin transport model utilizing the drift-diffusion approximation[12,13] shows that $\boldsymbol{\tau}_{\text{DL}}$ is related to $\text{Re}(g^{\uparrow\downarrow})$ while $\boldsymbol{\tau}_{\text{FL}}$ is proportional to $\text{Im}(g^{\uparrow\downarrow})$. The existence of $\boldsymbol{\tau}_{\text{FL}}$ has been confirmed in a wide range of FM/HM bilayers by various experimental methods with its magnitude as well as the sign depending on the details of the device structure (Table 2 of ref 11 and refs 14, 15).

Received: November 5, 2025
Revised: February 13, 2026
Accepted: February 18, 2026
Published: February 20, 2026



ACS Publications
© 2026 The Authors. Published by American Chemical Society

https://doi.org/10.1021/acs.nanolett.5c05536
Nano Lett. 2026, 26, 2853−2860

Downloaded from pubs.acs.org/naletd/article-pdf/26/8/2853/6382101/nl5c05536.pdf by UNIV REGENSBURG user on 11 November 2026

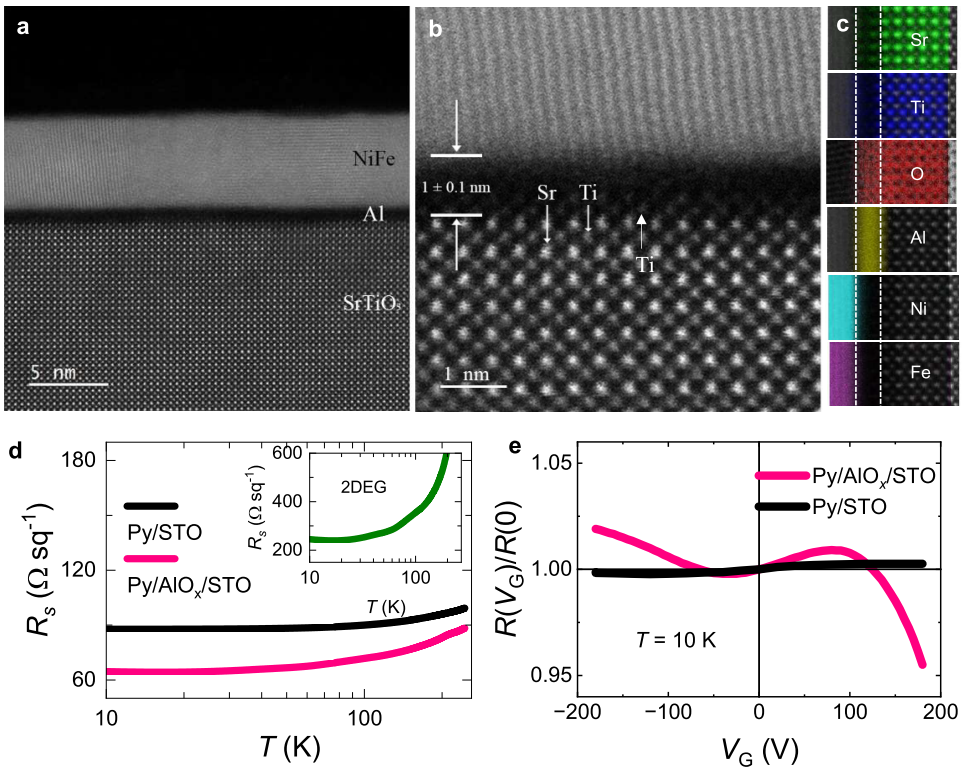


Figure 1. (a) HRTEM image of the Py/AlO_x/STO multilayers. (b) Magnified view of the Py/AlO_x and AlO_x/STO interfaces. (c) HAADF-STEM image and EDX of each element. (d) Temperature dependence of the sheet resistance of Py/AlO_x/STO (red line) and Py/STO (black line); the resistance of AlO_x/STO 2DEG is shown in the inset by the green line. (e) Gate-voltage V_G dependence of $R(V_G)/R(0)$ for Py/STO and Py/AlO_x/STO measured at 10 K.

Therefore, this indicates that $\mathrm{Im}(g^{\uparrow\downarrow})$ is sizable and the modulation of the gyromagnetic ratio due to $\mathrm{Im}(g^{\uparrow\downarrow})$ in spin pumping experiments cannot be ignored. So far, there are no experimental reports for the detection of the modulation of the g-factor by spin pumping in FM/HM bilayers, possibly because it is hard to detect the ferromagnetic resonance (FMR) of ultrathin FM with significantly enhanced α_{eff}.

Recently, a linear t^{-1}–g_{eff} behavior is found in a series of ultrathin Fe films grown on GaAs(001) substrate where a quasi two-dimensional electron gas (2DEG) forms at the Fe/GaAs interface.[16] This indicates that spin pumping leads to the modulation of g_{eff} (Supplementary Note 2). Surprisingly, the magnitude of $\mathrm{Im}(g^{\uparrow\downarrow})$ is about one order larger than $\mathrm{Re}(g^{\uparrow\downarrow})$, which indicates that the spin transport in the z-direction of the FM/2DEG system differs significantly from the diffusive spin transport in FM/HM bilayers with finite spin-diffusion lengths.[4−8] Although the mixing conductance in FM/2DEG bilayers has not been described theoretically, the preliminary results suggest that FM/2DEG could be ideal systems to study the modification of g_{eff} by spin pumping. In this work, we show that spin pumping can also lead to a significant modulation of the g-factor in another FM/2DEG system, i.e., the 2DEG at the AlO_x/$SrTiO_3$ interface with strong SOI. Specifically, we observe an anisotropic g-factor with 2-fold symmetry below the onset temperature of the 2DEG and a back gate-voltage even tunes this anisotropy by changing the Fermi level of the 2DEG.

To observe the modification of the Landé g-factor, we revisit the spin pumping experiments in Py/Al/STO multilayers.[17,18] Previous studies have demonstrated that depositing ultrathin Al on STO extracts oxygen from insulating Ti^{4+} ions in the STO substrate, creating electron-rich Ti^{3+} and/or Ti^{2+} states.[19] This process oxidizes the Al layer into AlO_x (hereafter referred to as Py/AlO_x/STO), while simultaneously forming a 2DEG at the AlO_x/STO interface, more accurately, within the first atomic planes of the STO surface. Angle-resolved photoemission spectroscopy (ARPES) studies confirm that even a 0.2 nm Al layer suffices to create this 2DEG.[19] Consequently, the AlO_x/STO system has emerged as a versatile platform for studying magnetism, superconductivity, and SOI, akin to the well-known 2DEG at the $LaAlO_3$/STO interface.[20] The surface-proximity of STO-based 2DEG makes it particularly suitable for spin injection experiments such as spin pumping. Recent experiments have revealed an exceptionally large spin-to-charge conversion efficiency at the AlO_x/STO,[17,18] the LAO/STO,[21] and $LaTiO_{3+\delta}$/STO interfaces,[22] which is ascribed to the large SOI and the enhanced momentum relaxation time in the 2DEG. Subsequent calculations by Johansson et al. further suggest that both spin-Rashba effect and orbital Rashba effect (ORE) contribute to the conversion, with ORE potentially dominating by at least an order of magnitude.[23] The existence of ORE has been demonstrated by the measurement of the anisotropic spin Seebeck voltage in Py/LAO/STO multilayers, in which the anisotropic spin Seebeck voltage is interpreted through the interplay between the anisotropic spin-to-charge and the isotropic orbit-to-charge conversion mechanisms.[24]

We grow AlO_x (6 nm)/Py ($Ni_{80}Fe_{20}$, 6 nm)/Al (1 nm) multilayers on STO (001) substrate by molecular-beam-epitaxy (Supplementary Note 1). Prior to growth, the substrate is heated in a vacuum up to 700 °C for 10 min. To minimize interdiffusion and especially agglomeration of Al, the substrate

Downloaded from pubs.acs.org/nalefd/article-pdf/26/8/2853/6382101/nl5c05536.pdf by UNIV REGENSBURG user on 11 November 2026

https://doi.org/10.1021/acs.nanolett.5c05536
Nano Lett. 2026, 26, 2853−2860

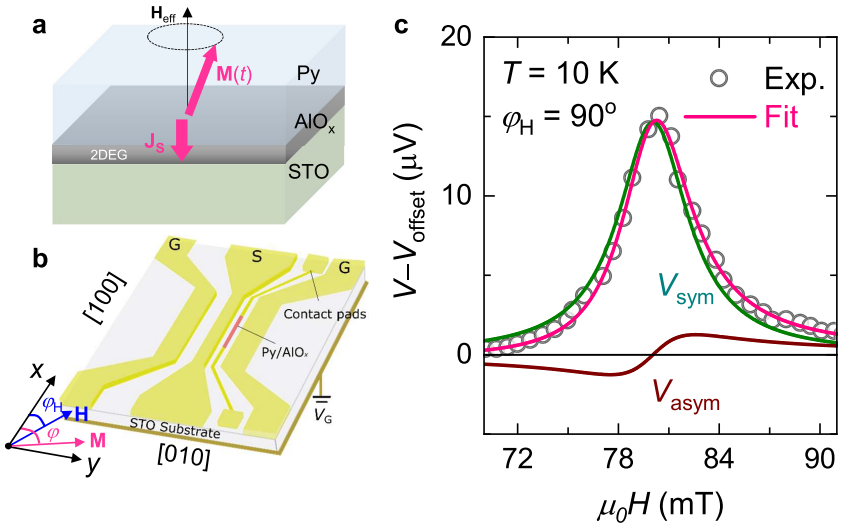


Figure 2. (a) Schematic of spin pumping from Py into the AlO_x/STO 2DEG. (b) Schematic of spin pumping device. φ_H (φ) is the angle of the magnetic-field **H** (the magnetization **M**). (c) Typical dc voltage spectra measured at T = 10 K, f = 8 GHz, and φ_H = 90°. The solids are the Lorentz fits.

temperature is further cooled below −140 °C when we deposit the Al and Py layers. Finally, a 6 nm AlO_x capping layer is deposited to avoid oxidation of Py. High-resolution transmission electron microscopy (HRTEM) (Figure 1a) and high-angle annular dark field scanning transmission electron microscopy (HAADF-STEM) (Figure 1b) images show that the Py/Al and Al/STO interfaces are sharp and flat, with no significant interdiffusion of atoms. The STO surface is terminated by Ti atoms, and the thickness of the AlO_x layer is estimated to be ∼ 1 ± 0.1 nm, slightly thinner than that expected from 1 nm Al deposition and its volume expansion by oxidation. The energy-dispersive X-ray (EDX) images (Figure 1c) show that oxygen has extended to the Al layer, and thus Al is oxidized to AlO_x.

Figure 1d shows the temperature (T) dependence of the resistance for Py/AlO_x/STO and Py/STO, in which a drop of the resistance is observed around 100 K for Py/AlO_x/STO. The extracted resistance of the 2DEG by the parallel resistance model shows the onset of the 2DEG around 100 K. Figure 1e presents the resistance measured by back gate-voltage V_G tuning, showing that the resistance of Py/STO is almost independent of V_G, while for Py/AlO_x/STO a sizable modulation is observed. These results further confirm the presence of a 2DEG for Py/AlO_x/STO. Note that an unusual V_G-dependence of resistance is observed for −50 V < V_G < +80 V for both samples; the resistance slightly increases as V_G increases. The reason for this reproducible behavior is unclear to us, and it has not been reported before.

For FMR measurements, we fabricate 7 μm × 320 μm Py/AlO_x/STO stripes integrated into the gap between the signal and ground lines of a coplanar waveguide (CPW) (Figure 2b). Under microwave excitation, the dc voltage spectrum $V(H)$ induced by FMR is measured while sweeping the magnetic-field H. Figure 2c shows typical $V(H)$ trace measured at the magnetic-field angle φ_H = 90°, at a microwave frequency f of 8 GHz, and T of 10 K. The spectrum is well-fitted by a combination of a symmetric ($L_{sym} = \Delta H^2/[4(H-H_R)^2 + \Delta H^2]$) and an antisymmetric ($L_{a\text{-}sym} = -4\Delta H(H-H_R)/[4(H-H_R)^2 + \Delta H^2]$) Lorentzian, i.e., $V-V_{offset} = V_{sym}L_{sym} + V_{a\text{-}sym}L_{a\text{-}sym}$. Here H_R is the resonance field, ΔH the full width at half-maximum, V_{offset} the offset voltage, and V_{sym} ($V_{a\text{-}sym}$) the symmetric (antisymmetric) component of the dc voltage. Here, $V_{a\text{-}sym}$ arises solely from the anisotropic magneto-resistance (AMR) effect of Py, while V_{sym} contains additional contributions from the spin pumping voltage induced by the inverse spin Rashba-Edelstein effect at the AlO_x/STO interface. Note that since the direction of detection of the d.c. voltage is parallel to the microwave current, the dynamic tunneling anisotropic magneto-resistance effect[25] and the dynamic Hanle effect,[26] which are detectable in a geometry transverse to the microwave current, cannot contribute to the signal. Before, we have shown that, for Si[27] and GaAs[28] substrates with low dielectric constant, the out-of-plane Oersted field induced by the rf current flowing in the CPW is the dominating excitation for magnetization dynamics, and it is possible to separate spin pumping voltages from AMR, while for STO substrate with large dielectric constant (∼20000 at 10 K), this separation becomes impossible for most of the measured gate-voltages because the in-plane excitation induced by the shunting current flowing in STO dominates (ref 29 and Supplementary Note 3). Below, we primarily focus on the discussion of H_R, which has largely been overlooked in spin pumping experiments.

Figure 3a shows the φ_H-dependence of H_R measured at f = 8 GHz for T = 120 K, 80K, 50, and 20 K. At 120 K, the H_R trace exhibits a clear uniaxial anisotropy with the minimum values (H_R^{min} ∼ 74.2 mT) occurring when **H** is parallel to the stripe (φ_H = 0° and 180°, easy axis) and with maximum values (H_R^{max} ∼ 76.6 mT) occurring when **H** is perpendicular to the stripe (φ_H = 90° and 270°, hard axis). This 2-fold symmetry of H_R is well-described by the resonance condition,[30]

$$\left(\frac{2\pi f}{\gamma}\right)^2 = \mu_0^2 H_1 H_2 \tag{4}$$

where $H_1 = H_R \cos(\varphi-\varphi_H) + H_K + H_U \cos^2\varphi$, $H_2 = H_R \cos(\varphi-\varphi_H) + H_U \cos 2\varphi$, φ the angle of **M**, H_K the effective demagnetization anisotropy field, and H_U the uniaxial shape anisotropy field. From the fits, the values of g, H_K, and H_U are respectively determined to be 2.1, 914, and 0.87 mT. The magnitude of H_K matches the saturation magnetization of Py, i.e., $H_K \sim N_{zz}M$, where N_{zz} is the out-of-plane demagnetizing

https://doi.org/10.1021/acs.nanolett.5c05536
Nano Lett. 2026, 26, 2853−2860

Downloaded from pubs.acs.org/naletd/article-pdf/26/8/2853/6382101/nl5c05536.pdf by UNIV REGENSBURG user on 11 November 2026

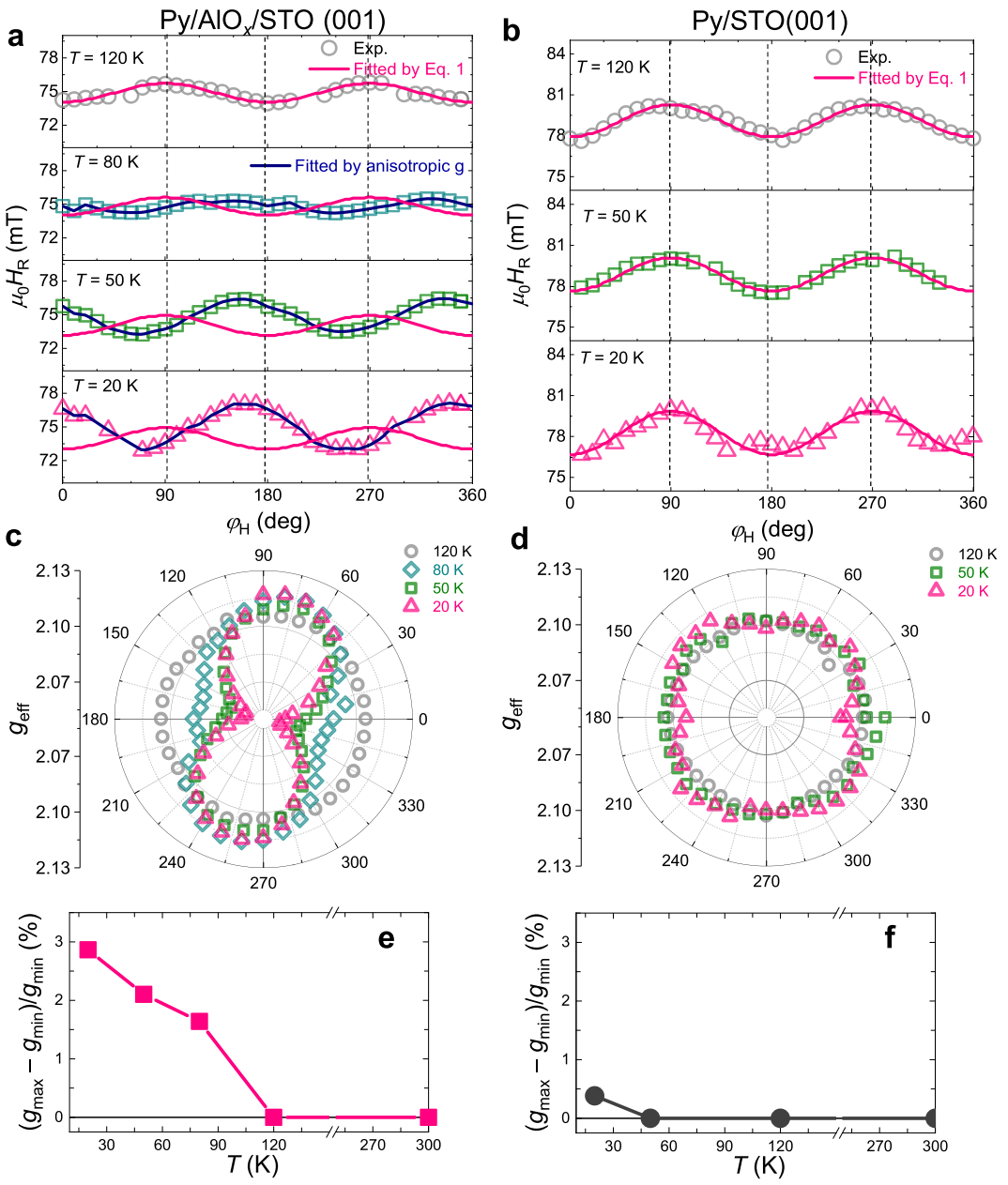


Figure 3. (a) φ_H-dependence of the resonance field H_R of the Py/AlO$_x$/STO sample measured at f = 8 GHz and T = 120 K, 80 K, 50 K, and 20 K. (b) φ_H-dependence of H_R of the Py/STO sample measured at f = 8 GHz and T = 120 K, 50 K, and 20 K. The pink lines in (a) and (b) are calculated by eq 4 using the shape anisotropy of the stripe, and the blue lines in (a) are calculated by considering anisotropic g-factor. (c) Polar plot of the anisotropic Landé g-factors for the Py/AlO$_x$/STO samples at different temperatures. (d) Polar plot of the g-factors for the Py/STO samples at different temperatures. (e) and (f) T-dependence of the g-anisotropy, $(g^{max}-g^{min})/g^{min}$, for Py/AlO$_x$/STO and for Py/STO.

factor, confirming its dominant origin from thin-film demagnetization with negligible perpendicular anisotropy at the Py/AlO$_x$ interface. Similarly, H_U quantitatively matches the anisotropy field induced by the shape of the Py stripe, i.e., $H_U \sim N_{yy}M$, where N_{yy} is the in-plane demagnetizing factor perpendicular to the stripe (Supplementary Note 4).

As T is decreased to 80 K (i.e., below the onset temperature for the 2DEG), the angular trace of H_R differs significantly from that obtained at 120 K: H_R^{min} now appears at 75° (255°) and H_R^{max} at 165° (345°). This phase shift persists down to 20 K with an enhanced H_R^{max}-H_R^{min} value of 4 mT. Obviously, the unusual angular trace of H_R at lower temperatures, which has been reproduced by several other stripe- and full-film- samples (Supplementary Note 5), cannot be explained by considering the uniaxial shape anisotropy of the stripe (pink lines). To exclude any possibility that the shift of H_R arises from an unknown magnetic anisotropy induced by the STO substrate, we additionally prepared a Py (6 nm)/STO bilayer and performed similar measurements. As shown in Figure 3b, no shift of H_R is observed for all measured temperatures, i.e., H_R^{min} (H_R^{max}) appears for φ_H = 0° and 180° (φ_H = 90° and 270°), and all the H_R-traces can be well-fitted by eq 4 using the shape anisotropy of the stripe rather than by additional magnetic anisotropies induced by the STO substrate. Moreover, all the samples studied here are capped by AlO$_x$, and thus any unknown effect from the Py/AlO$_x$ interface can also be excluded.

https://doi.org/10.1021/acs.nanolett.5c05536
Nano Lett. 2026, 26, 2853−2860

Downloaded from pubs.acs.org/nalefd/article-pdf/26/8/2853/6382101/4/nl5c05536.pdf by UNIV REGENSBURG user on 11 November 2026

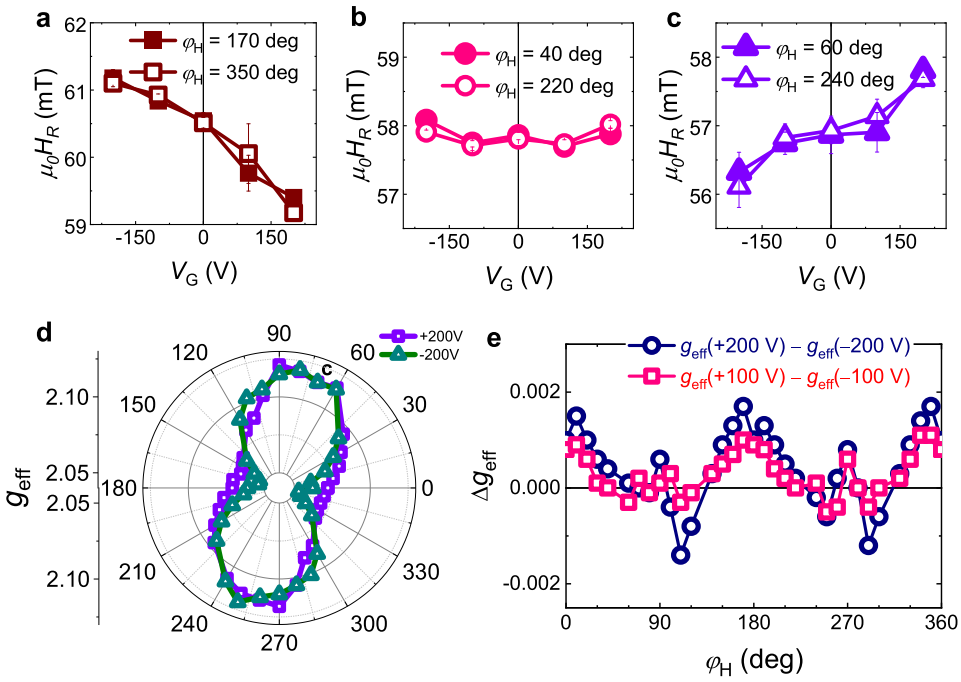


Figure 4. (a), (b), and (c): V_G-dependence of H_R for Py/AlO$_x$/STO measured at f = 7 GHz and T = 10 K for φ_H = 170°/350°, φ_H = 40°/220°, and φ_H = 60°/240°. (d) Polar plot of the anisotropic g-factor values for V_G = −200 V and +200 V. (f). φ_H-dependence of Δg, where $\Delta g(\pm V_G)$ = $g(+V_G)-g(-V_G)$.

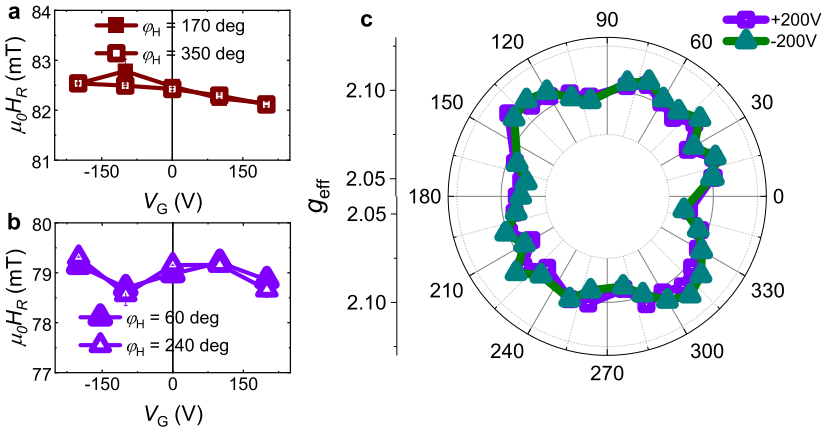


Figure 5. (a) and (b): V_G-dependence of H_R for Py/STO measured at f = 8 GHz and T = 10 K for φ_H = 170°/350° and φ_H = 60°/240°. (c) Polar plot of the corresponding g-factor values for V_G = −200 V and +200 V.

Therefore, the observed H_R-trace phase shift in the Py/AlO$_x$/STO device must be interpreted in terms of an anisotropic Landé g-factor induced by spin pumping. By measuring the frequency-dependence of H_R at fixed φ_H angles (Supplementary Note 6) and fitting with eq 4 (fixing H_K and H_U values while varying g), a clear 2-fold symmetry of the g-factor is obtained at T = 50 K and 20 K. The minimum g^{min} appears at 165° (345°) while the maximum g^{max} appears at 75° (255°) (Figure 3c), and the relative anisotropy $(g^{max}-g^{min})/g^{min}$ increases as T decreases (Figure 3e). In contrast, the Py/STO control sample shows nearly isotropic g-values at T = 120 and 50 K (Figure 3d), and the relative anisotropy $(g^{max}-g^{min})/g^{min}$ shows weak increases as T decreases (Figure 3f). For T = 20 K, a weak 2-fold anisotropy is observed, which could be related to the emergence of a weaker 2DEG at the Py/STO interface[31] (one may also note a weak 4-fold symmetry in Figure 3d. However, due to its weakness, it is difficult to clearly identify.).

To verify that the angular momentum absorption by the 2DEG at the AlO$_x$/STO interface indeed plays a role for the shift of H_R, we insert a 4 nm Pt layer between Py and STO as an isotropic spin sink and perform the same measurements as the Py/AlO$_x$/STO and the Py/STO samples. As shown in Figure S9, the Pt insertion completely suppresses the unusual H_R-shift, and all the H_R traces can be interpreted by the uniaxial shape anisotropy of the Py stripe with an isotropic g-factor. This confirms again that the emergence of the anisotropic g-factor in Py/AlO$_x$/STO is related to spin pumping into 2DEG and is not from any unknown magnetic anisotropies induced by the substrate.

The exceptionally large dielectric constant[32] of STO combined with the 2DEG's low carrier density enables effective Fermi level tuning via back gate-voltage, as evidenced

Downloaded from pubs.acs.org/naletd/article-pdf/26/8/2853/6382101/nl5c05536.pdf by UNIV REGENSBURG user on 11 November 2026

https://doi.org/10.1021/acs.nanolett.5c05536
Nano Lett. 2026, 26, 2853−2860

by the sizable modulation of the resistance (Figure 1e). Here, we address the influence of V_G on H_R and thus on the anisotropic g-factor. Figure 4a-4c shows the V_G-dependence of H_R measured at f = 7 GHz and T = 10 K for different magnetic-field angles. For φ_H = 170° and 350° (Figure 4a), H_R decreases with V_G and the modulation of H_R is about −2 mT; for φ_H = 40° and 220° (Figure 4b), H_R is almost independent of V_G; however, for φ_H = 60° and 240° (Figure 4c), H_R increases with V_G and the modulation of H_R is about +2 mT. This φ_H-dependence of the H_R response indicates that the modulation of H_R does not originate from the change of magnetic anisotropies of Py by V_G via the magnetoelectric effect[33] (Supplementary Note 11), since: I) the electric-field primarily affects the 2DEG rather than the Py film, and the magnetic properties of Py can be hardly modified by V_G because of its high carrier concentration (~10^{23} cm^{-3}), II) If there were a modulation of H_K and/or H_U by V_G, the dependence of H_R on V_G should be independent of φ_H.

Figure 4d summarizes the φ_H-dependent g-value anisotropy for V_G = +200 V and +200 V. The g-factor shows an anisotropic modification, i.e., for φ_H = 170° and 350° g(+200 V) < g(+200 V) holds; for φ_H = 40° and 220° g(+200 V) ~ g(−200 V) holds; while for φ_H = 60° and 240°, g(+200 V) > g(+200 V) holds. The gate-tunable anisotropy becomes more pronounced when $\Delta g(\pm V_G) = g(+V_G)\text{-}g(-V_G)$. As shown in Figure 4e, $|\Delta g(\pm 200\ V)| > |\Delta g(\pm 100\ V)|$ holds, and Δg changes sign several times when φ_H varies from 0° to 360°, indicating that Δg is also anisotropic. Control measurements on Py/Pt/STO and Py/STO samples (Supplementary Notes 9 and 10) show no modulation for the former and significantly weaker modulation for the latter (Figure 5), confirming that the anisotropic g-factor tuning in the Py/AlO_x/STO sample originates from the modulation of the Fermi level of the 2DEG.

Under FMR, the magnetization precession in the polycrystalline Py layer injects spin currents into the 2DEG (Figure 2a), and the injected spin currents are isotropic. However, if the spin sink is anisotropic, this can lead to the emergence of an anisotropic g-factor. Previous theoretical and experimental studies have shown that the anisotropic spin textures for the STO-based 2DEG show a 4-fold symmetry.[23,24] Therefore, this should lead to a 4-fold symmetry of the anisotropic g-factor which cannot explain the 2-fold symmetry as observed in the experiments. On the other hand, the pristine STO is an insulating cubic perovskite with a lattice constant of 3.905 Å when T > 105 K. Below 105 K, STO undergoes the cubic-to-tetragonal structural phase transition,[34,35] accompanied by a broken in-plane rotation symmetry[36] with $a < b < c$, where a and b are the lattice constants in the (100) plane of the tetragonal structure, and c is the lattice constant along [001]. A *local* scanning tunneling microscopy characterization reveals that this broken rotational symmetry is more significant and an enhanced b/a up to 1.19.[37] Over a wide range of surface oxygen vacancies, the broken rotational symmetry leads to weakly unidirectional electronic states, mostly aligned along the [110]-direction. Moreover, ARPES measurements can also not exclude this weak anisotropy.[17,19,38] Since the mixing conductance is expressed in terms of spin-dependent reflection and transmission coefficients for electronic states at the interface[2,4] and the reflection and transmission coefficients should be proportional to the density of states at Fermi level, the emergence of 2-fold anisotropic g-factor could be induced by the anisotropic density of states at the 2DEG. Therefore, we infer that the unidirectional electronic states may be responsible for the observed 2-fold anisotropic g-factor at low temperatures, where the angular momentum absorption efficiency is enhanced due to an increase of the momentum relaxation time. On the other hand, the broken rotational symmetry may induce Dresselhaus SOI, and the interplay of Rashba and Dresselhaus terms could account for our observations. Additional experimental and theoretical work is needed to confirm the Dresselhaus SOI in STO systems.

It is known that one of the hallmarks of spin pumping measurements in heavy metal/FM bilayers is the enhancement of the Gilbert damping value compared to that of the single FM.[2,3] In principle, if the spin sink has an anisotropic electronic texture at the Fermi level, both an anisotropic damping[39,40] and an anisotropic g-factor should be observed. However, our results show that, within experimental accuracy, the damping is almost isotropic and independent of V_G (Supplementary Notes 8, 9, and 10). One reason for this is the coexistence of orbital pumping.[24,41−43] Previous studies have shown that the magnitude of spin moment for AlO_x/STO 2DEG is much smaller than the orbital moment,[23,24] and this leads to less damping enhancement from the loss of spin angular momentum of Py and an insensitivity to V_G. Moreover, the relatively small orbit-to-spin magnetization ratio in Py limits the orbital-current flow into the 2DEG, reducing the orbital pumping contribution to the damping.[44] However, because of the significant shunting current in STO, it is not possible to accurately separate the orbital pumping voltage from the symmetric AMR effect (Supplementary Note 3).

Our results show a clear gyromagnetic ratio modulation in FMR pumping experiments. The effect has been theoretically predicted for a long time,[2] but the experimental detection was still missing.[16] We note that a quantitative understanding of the anisotropic modulation by gate-voltage, which could arise from the competition of various Fermi-energy-dependent effects, e.g., the anisotropic electron density or the interplay between spin angular momentum and orbital angular momentum absorption, is still elusive. We also note that a sign reversal of the Rashba coefficient has been observed in several STO-based 2DEGs,[17,18,21,22,24] and it is unclear for us how to connect the g-factor modulation with the Rashba-SOI. The discrepancy between the g-factor modulation and the Rashba coefficient modulation might arise from the fact that the g-factor is related to Im $(g^{\uparrow\downarrow})$ while the extracted Rashba coefficient is related to Re $(g^{\uparrow\downarrow})$. Qualitative and quantitative theory are still missing so far. The emergence of the anisotropic g-factor results from spin pumping in the presence of an anisotropic electronic distribution. The modulation of the gyromagnetic ratio in FMR pumping experiments highlights its potential as a probe for the imaginary part of mixing conductance in an FM/2DEG system. The modulation is not limited through the spin-charge and orbital-charge conversion processes. Their inverse processes, i.e., current-induced angular momentum accumulation, can also lead to a modulation of the g-factor and magnetism.[45] These findings bridge a critical gap between theory and experiment, offering new avenues to manipulate magnetic properties in spin and orbitronic devices.

■ ASSOCIATED CONTENT

Supporting Information

The Supporting Information is available free of charge at https://pubs.acs.org/doi/10.1021/acs.nanolett.5c05536.

Downloaded from pubs.acs.org/naleld/article-pdf/26/8/2853/6382014/nl5c05536.pdf by UNIV REGENSBURG user on 11 November 2026

https://doi.org/10.1021/acs.nanolett.5c05536
Nano Lett. 2026, 26, 2853−2860

Methods, Mixing conductance in Fe/GaAs quasi two-dimensional system, Spin pumping voltage in Py/AlOx/STO multilayers, Quantifying the shape anisotropy of the Py stripe, Angular dependence of H_R for other Py/AlOx/STO samples, Frequency dependence of H_R in Py/AlOx/STO and Py/STO devices, Isotropic g-factor in Py/Pt/STO, Angular- and temperature-dependence of damping in Py/AlOx/STO, Py/STO and Py/Pt/STO, V_G-dependence of damping in Py/AlOx/STO, V_G-dependence of resonance field and damping in Py/Pt/STO and Py/STO, Excluding the charge mediated magnetoelectric coupling effect in gate modulation of measurement (PDF)

AUTHOR INFORMATION

Corresponding Authors

Weiwei Zhao − *Sauvage Laboratory for Smart Materials, School of Integrated Circuit, Harbin Institute of Technology, Shenzhen 518055, China;* orcid.org/0000-0002-0373-1146; Email: wzhao@hit.edu.cn

Lin Chen − *Department of Physics and Center for Quantum Engineering (ZQE), Technical University of Munich, 85748 Garching b. Munich, Germany;* orcid.org/0000-0002-8233-800X; Email: lin0.chen@tum.de

Authors

Jian Shao − *Sauvage Laboratory for Smart Materials, School of Integrated Circuit, Harbin Institute of Technology, Shenzhen 518055, China; Department of Physics, Technical University of Munich, 85748 Garching b. Munich, Germany*

Matthias Kronseder − *Institute of Experimental and Applied Physics, University of Regensburg, 93049 Regensburg, Germany*

Jianping Guo − *Department of Physics and Center for Quantum Engineering (ZQE), Technical University of Munich, 85748 Garching b. Munich, Germany*

Maximilian Mangold − *Department of Physics and Center for Quantum Engineering (ZQE), Technical University of Munich, 85748 Garching b. Munich, Germany;* orcid.org/0009-0008-2809-1852

Dong Pan − *State Key Laboratory of Semiconductor Physics and Chip Technologies, Institute of Semiconductors, Chinese Academy of Science, Beijing 100083, China;* orcid.org/0000-0003-2067-6983

Thomas N. G. Meier − *Department of Physics and Center for Quantum Engineering (ZQE), Technical University of Munich, 85748 Garching b. Munich, Germany*

Jianhua Zhao − *State Key Laboratory of Semiconductor Physics and Chip Technologies, Institute of Semiconductors, Chinese Academy of Science, Beijing 100083, China; National Key Laboratory of Spintronics, Hangzhou International Innovation Institute, Beihang University, 11115 Hangzhou, China*

Christian H. Back − *Department of Physics and Center for Quantum Engineering (ZQE), Technical University of Munich, 85748 Garching b. Munich, Germany; Munich Center for Quantum Science and Technology (MCQST), 80799 Munich, Germany;* orcid.org/0000-0003-3840-0993

Complete contact information is available at: https://pubs.acs.org/10.1021/acs.nanolett.5c05536

Author Contributions

M.K. initialized the project about STO. L.C., W. Z., and C.H.B supervised the study. J.S. and J.P.G fabricated the device. J.S., J.P.G., L.C., and M.M. collected the data, which was analyzed by J.S. and L.C. M.K. and T.N.G.M. grew the samples. P.D. and J.H.Z. carried out the HRTEM measurements. L.C. wrote the manuscript with input from all authors. All authors discussed the results and provided comments on the manuscript.

Notes

The authors declare no competing financial interest.

ACKNOWLEDGMENTS

The authors thank C. Gorini, M. Viret, and A. Smogunov for fruitful discussions. This work was funded by the Deutsche Forschungsgemeinschaft by TRR 360-492547816 and SFB1277-314695032, by the excellence cluster MCQST under Germany's Excellence Strategy EXC-2111 (Project no. 390814868), by the Natural Science Foundation of China No. 52073075, and Shenzhen Science and Technology Program (Grant No. KQTD20170809110344233). J. Guo and J. Shao were partially supported by the China Scholarship Council (CSC).

REFERENCES

(1) Gilbert, T. L. A Phenomenological theory of damping in ferromagnetic materials. *IEEE Trans. Magn.* **2004**, *40*, 3443−3449.

(2) Tserkovnyak, Y.; et al. Enhanced Gilbert damping in thin ferromagnetic films. *Phys. Rev. Lett.* **2002**, *88*, No. 117601.

(3) Mizukami, S.; et al. Effect of spin diffusion on Gilbert damping for very thin permalloy layer in Cu/permalloy/Cu/Pt films. *Phys. Rev. B* **2002**, *66*, No. 104413.

(4) Zwierzycki, S.; et al. First principles study of magnetization relaxation and spin transfer in thin magnetic films. *Phys. Rev. B* **2005**, *71*, No. 064420.

(5) Xia, K.; et al. Spin torques in ferromagnetic/normal-metal structures. *Phys. Rev. B* **2002**, *65* (R), No. 220401.

(6) Carva, K.; Turek, I. Spin mixing conductances in thin magnetic films from first principles. *Phys. Rev. B* **2007**, *76*, No. 104407.

(7) Zhang, Q.; Hikino, S.-i.; Yunoki, S. First-principles study of the spin mixing conductance in $Pt/Ni_{81}Fe_{19}$ junctions. *Appl. Phys. Lett.* **2011**, *99*, No. 172105.

(8) Dolui, K.; et al. Effective spin mixing conductance of topological-insulator/ferromagnet and heavy-metal/ferromagnet spin-orbit-coupled interfaces: A first-principle Floquet-nonequilibrium Green function approach. *Phys. Rev. Mater.* **2020**, *4* (R), No. 121201.

(9) Petitjean, C.; Luc, D.; Waintal, X. Unified drift-diffusion theory for transverse spin currents in spin valves, domain walls, and other textured magnets. *Phys. Rev. Lett.* **2012**, *109*, No. 107204.

(10) Taniguchi, T.; et al. Determination of penetration depth of transverse spin current in ferromagnetic metals by spin pumping. *Appl. Phys. Expre.* **2008**, *1*, No. 031302.

(11) Manchon, A.; et al. Current-induced spin-orbit torques in ferromagnetic and antiferromagnetic systems. *Rev. Mod. Phys.* **2019**, *91*, No. 035004.

(12) Haney, P. M.; et al. Current induced torques and interfacial spin-orbit coupling: Semiclassical modeling. *Phys. Rev. B* **2013**, *87*, No. 174411.

(13) Pai, C. F.; et al. Dependence of efficiency of spin Hall torque on the transparency of Pt/ferromagnetic layer interfaces. *Phys. Rev. B* **2015**, *92*, No. 064426.

(14) Chen, L.; et al. Connections between spin-orbit torques and unidirectional magnetoresistance in ferromagnetic-metal-heavy-metal heterostructures. *Phys. Rev. B* **2022**, *105*, No. L020406.

Downloaded from pubs.acs.org/naleld/article-pdf/26/8/2853/6382101/nl5c05536.pdf by UNIV REGENSBURG user on 11 November 2026

(15) Krishnia, S.; et al. Large interfacial Rashba interaction generating strong spin−orbit torques in atomically thin metallic heterostructures. *Nano Lett.* **2023**, *23*, 6785−6791.
(16) Chen, L.; et al. Interfacial tuning of anisotropic Gilbert damping. *Phys. Rev. Lett.* **2023**, *130*, No. 046704.
(17) Vaz, D.; et al. Mapping spin-charge conversion to the band structure in a topological oxide two-dimensional electron gas. *Nat. Mater.* **2019**, *18*, 1187−1193.
(18) Noël, P.; et al. Non-volatile electric control of spin−charge conversion in a SrTiO3 Rashba system. *Nature* **2020**, *580*, 483−486.
(19) Rödel, T.; et al. Universal fabrication of 2D electron systems in functional Oxides. *Adv. Mater.* **2016**, *28*, 1976−1980.
(20) Ohtomo, A.; et al. A high-mobility electron gas at the $LaAlO_3$/$SrTiO_3$ heterointerface. *Nature* **2004**, *427*, 423−426.
(21) Lesne, E.; et al. High efficient and tunable spin-to-charge conversion through Rashba coupling at oxide interfaces. *Nat. Mater.* **2016**, *15*, 1261−1266.
(22) Kaneta-Takada, S.; Kitamura, M.; Arai, S.; et al. Giant spin-to-charge conversion at an all-epitaxial single-crystal-oxide Rashba interface with a strongly correlated metal interlayer. *Nat. Commun.* **2022**, *13*, 5631.
(23) Johansson, A.; et al. Spin and orbital Edelstein effects in a two-dimensional electron gas: Theory and application to $SrTiO_3$ interface. *Phys. Rev. Res.* **2021**, *3*, No. 013275.
(24) El Hamdi, A.; et al. Observation of the orbital inverse Rashba−Edelstein effect. *Nat. Phys.* **2023**, *19*, 1855−1860.
(25) Liu, C.; et al. Electrical detection of ferromagnetic resonance in ferromagnet/n-GaAs heterostructures by tunneling anisotropic magnetoresistance. *Appl. Phys. Lett.* **2014**, *105*, No. 212401.
(26) Liu, C.; Patel, S.; Peterson, T.; et al. Dynamic detection of electron spin accumulation in ferromagnet−semiconductor devices by ferromagnetic resonance. *Nat. Commun.* **2016**, *7*, No. 10296.
(27) Obstbaum, M.; et al. Inverse spin Hall effect in $Ni_{81}Fe_{19}$/normal-metal bilayers. *Phys. Rev. B* **2014**, *89* (R), No. 060407.
(28) Chen, L.; et al. Robust spin-orbit torque and spin-galvanic effect at the Fe/GaAs (001) interface at room temperature. *Nat. Commun.* **2016**, *7*, No. 13802.
(29) Jiang, D.; et al. Substrate-induced spin-torque-like signal in spin-torque ferromagnetic resonance measurement. *s, Phys. Rev. Appl.* **2024**, *21*, No. 024021.
(30) Chen, L.; Matsukura, F.; Ohno, H. Direct-current voltages in (Ga,Mn)As structures induced by ferromagnetic resonance. *Nat. Commun.* **2013**, *4*, 2055.
(31) Posadas, A. B.; et al. Scavenging of oxygen from $SrTiO_3$ during oxide thin film deposition and the formation of interfacial 2DEGs. *J. Appl. Phys.* **2017**, *121*, No. 105302.
(32) Yang, Z.; et al. Epitaxial $SrTiO_3$ films with dielectric constants exceeding 25,000. *PNAS* **2022**, *119*, No. e2202189119.
(33) Zhou, Z.; et al. Quantifying thickness-dependent charge mediated magnetoelectric coupling in magnetic/dielectric thin film heterostructures. *Appl. Phys. Lett.* **2013**, *103*, No. 232906.
(34) Cowley, R. A. Lattice dynamics and phase transition of Strontium Titanate. *Phys. Rev.* **1964**, *134*, A981.
(35) Shirane, G.; et al. Lattice dynamical study of the 110 K phase transition in $SrTiO_3$. *Phys. Rev.* **1969**, *177*, 858.
(36) Lytle, F. W.; et al. X-ray diffractometry of low-temperature phase transformations in Strontium Titanate. *J. Appl. Phys.* **1964**, *35*, 2212−2215.
(37) Ding, C.; et al. Unidirectional charge orders induced by Oxygen vacancies on $SrTiO_3$(001). *ACS Nano* **2024**, *18*, 17786−17793.
(38) McKeown Walker, S.; et al. A laser-ARPES view of the 2D electron systems at $LaAlO_3$/$SrTiO_3$ and Al/$SrTiO_3$ interfaces. *Adv. Elect. Mater.* **2022**, *8*, No. 2101376.
(39) Chen, L.; Mankovsky, S.; Wimmer, S.; et al. Emergence of anisotropic Gilbert damping in ultrathin Fe layers on GaAs(001). *Nat. Phys.* **2018**, *14*, 490−494.
(40) Yang, X.; et al. Anisotropic nonlocal damping in ferromagnet/α-GeTe bilayers enhanced by splitting energy bands. *Phys. Rev. Lett.* **2023**, *131*, No. 186703.
(41) Go, D.; et al. Orbital pumping by magnetization dynamics in ferromagnets. *Phys. Rev. B* **2025**, *111* DOI: 10.1103/PhysRevB.111.L140409.
(42) Hayashi, H.; et al. Observation of orbital pumping. *Nat. Electron* **2024**, *7*, 646−652.
(43) Keller, N.; et al. Identification of orbital pumping from spin pumping and rectification effects. *Nano Lett.* **2025**, *25*, 13462−13467.
(44) Ding, S.; et al. Mitigation of Gilbert damping in the CoFe/CuO_x orbital torque system. *Nano Lett.* **2024**, *24*, 10251−10257.
(45) Lee, G.; Kim, K. W.; Lee, K. J. Orbital exchange-mediated current control of magnetism. *Nat. Commun.* **2026**, DOI: 10.1038/s41467-026-68846-x.

Downloaded from pubs.acs.org/nalefd/article-pdf/26/8/2853/6382101/nl5c05536.pdf by UNIV REGENSBURG user on 11 November 2026

https://doi.org/10.1021/acs.nanolett.5c05536
Nano Lett. 2026, 26, 2853−2860